2024 IEEE International Conference on Robotics and Automation (ICRA 2024)
May 13-17, 2024. Yokohama, Japan

Safe-By-Design Digital Twins for Human-Robot Interaction: A Use Case for Humanoid Service Robots

Jon Škerlj*, Mazin Hamad*,†, Jean Elsner, Abdeldjallil Naceri, and Sami Haddadin

***Abstract*— Integrating humanoid service mobile robots into human environments presents numerous challenges, primarily concerning the safety of interactions between robots and humans. To address these safety concerns, we propose a novel approach that leverages the capabilities of digital twin technology by tailoring it to incorporate comprehensive and robust safety concepts. This paper introduces a "safe-by-design" digital twin that operates alongside the real twin robot in the loop, engaging real-time safety framework during physical interactions with the surrounding environment, including humans.**

To validate the effectiveness of our proposed safe-by-design digital twin framework, we conducted experiments using a humanoid service mobile robot alongside simulated human counterparts. Our results demonstrate the capability of the integrated impact safety module within the proposed digital twin approach to limit the velocities of both the robot's base and arms, adhering to injury biomechanics-based safety thresholds. These findings emphasize the promise of our proposed approach for ensuring the physical safety of humanoid service mobile robots operating in dynamic human environments. It enables the digital twin to preemptively identify potential safety hazards and formulate safe intervention actions to ensure the robot's compliance with safety regulations, paving the way for safer and more widespread adoption of robotic systems in various service domains.

I. Introduction

According to the international standard for robotics vocabulary (ISO8373) [1], service robots are differentiated from industrial robots that have historically dominated the market. Unlike their industrial counterparts, which are typically engineered to execute a specific task repetitively in a controlled environment, service robots are expected to operate in dynamic and unpredictable settings alongside humans [2]. Personal service robots represent a distinct category of service robots designed to perform tasks beneficial to humans in domestic environments [3]. This necessitates capabilities such as interaction, learning, adaptation, and autonomous error correction to navigate the complexities of human environments effectively [4].

Service robots can further be classified in *affective* (or social) and *effective* (or utilitarian) based on their design strategies [5]. For instance, among the commercially available affective personal service robots is the humanoid robot *Pepper* [6], which was specifically designed for social interaction. Its child-like design, size, and form are positively received and well accepted by elderly users [7]. However, these robots usually have a limited payload, control and sensing capabilities, and are therefore unable to perform complex physical manipulation and interaction tasks with humans [8], see Fig. 1. Moreover, even though some safety standards and metrics for industrial collaborative robots [9]–[11] and personal care robots [12] exist today, it still seems inadequate for reaching the full potential of humanoid service robots. Substantial difficulties persist for mobile systems used in nonindustrial, unstructured environments in our everyday lives, potentially full of cluttered human interactions, making the occurrence of unexpected contacts and subsequent injury risk very probable [13]. However, a lot of promising research and developed work is currently being conducted in order to overcome these safety challenges [14], [15]. Furthermore, a redefinition of safety by introducing new dimensions (interaction, cyber, societal, and temporal) in order to consider additional aspects besides physical safety was proposed in [16]. This new definition aligns better with the risks of human-robot interaction and technological advancement in artificial intelligence and cyber-physical systems. Humanoid robots, which comprise a special class of personal service robots, can be seen as examples of such systems. Their final aim is to be deployed in an unknown environment to assist people and interact with them directly. Although many humanoid systems have been currently developed, they are primarily used as research platforms [17]–[24].

Fig. 1: An exemplary physical interaction scenario showcasing the humanoid robot GARMI and a human user. By synchronizing both the robot and human joint locations from the physical twin PT (left), physical interactions occurring in the real-world can be precisely mapped to the digital twin DT (right).

Current challenges facing humanoid robots

In contrast to the Pepper robot, more advanced humanoids face numerous challenges that hinder their accessibility to end users [25]. A primary obstacle in this regard is the absence of well-defined, unified safety approaches. At the moment, different safety strategies are applied by every individual robot. For instance, adding arbitrary limits on joint positions, velocities, and/or torques [23], monitoring the internal state of the platform [22], stopping all action if unexpected contact or force has been detected [21]–[23]. Unfortunately, just ensuring physical safety is not enough for service humanoids to enter the domestic arena. Additional high-level concerns from different perspectives, e.g., legal and ethical, need to be addressed. For example, complying with governmental data security regulations (e.g., GDPR in Europe) and clear accountability and transparency procedures [26], [27]. Additionally, medical device regulations could apply if the humanoid robot is used as a medical tool, e.g., for rehabilitation or tele-diagnostics [28].

*Shared first authorship; the two authors contributed equally.

All authors are with the Chair of Robotics and Systems Intelligence, Munich Institute of Robotics and Machine Intelligence, Department of Computer Engineering, School of Computation, Information and Technology, Technical University of Munich (TUM).

†Corresponding author. Email: mazin.hamad@tum.de

One technology that could potentially bridge the aforementioned research gap is the digital twin (DT) concept. Unfortunately, the use of the term DT has been vague in the literature of the last decade with many different definitions [29], [30]. A very elaborate overview discussion on the past, present, and future digital twins has been recently introduced in [31].

Up to now, the use of DT technology in service robotics and healthcare has not yet fully matured as compared to other industries such as assembly line manufacturing [32]. Manufacturing offers a controlled environment where the states of the physical system can be easily recorded and digitized. For instance, a digital model of the service humanoid Pepper was developed in [33] and used to train the model in the digital world to allow its physical twin (PT) to perform object-touching tasks. Nevertheless, until recently, most existing DT systems focused only on the technical system without considering humans in the equation. However, with the increased use of collaborative robots in manufacturing, human models are being added to the digital world [34]–[36] with the aim to increase the safety, ergonomics, and efficiency of the manufacturing process. To the best of the authors' knowledge, as of today no DTs exist in the service robotics sector for physical Human-Robot Interaction (pHRI) that represent both the robot and the human in the same digital domain and use that to improve their interaction. We think this research gap should be explored since it offers great potential to bridge service robots from the laboratories to a home setting.

Contribution

In this paper, similar to a recently proposed approach for cobotic workstations in [35], we develop a physically-consistent DT that has the following properties:

i) high fidelity multi-physics digital model capable of describing the micro and macro features and mirroring the state of and the behavior of the physical system,
ii) capability of performing simulation in the virtual model and mirroring the same to the physical model in real-time, and
iii) employing a two-way real-time communication for data transfer between the physical and the digital systems.

Our scientific contributions can be summarized as follows:

I. We propose a novel safe-by-design DT framework for pHRI to speed up the process of application prototyping for service humanoids operated in domestic environments shared with humans (see Fig. 2),
II. Accounting for high-level concerns from ethical and legal perspectives, the proposed DT framework fulfills the requirements of data recording and compliance with GDPR for service mobile robots,
III. By employing accurate physical models, it is capable of capturing the contact dynamics arising from the movement of different parts of its robotic systems (including robot-to-human impacts),
IV. Relying on a multi-layered safety architecture guiding the generation of simulated task/motion plans and control actions, human kinematics and musculoskeletal models can be used within our DT to ensure safe pre-collision control of robots in pHRI applications.
V. For validation, we demonstrate its ability to address impact safety during pHRI by implementing a pain/injury biomechanics based data-driven safety approach for pre-collision control.

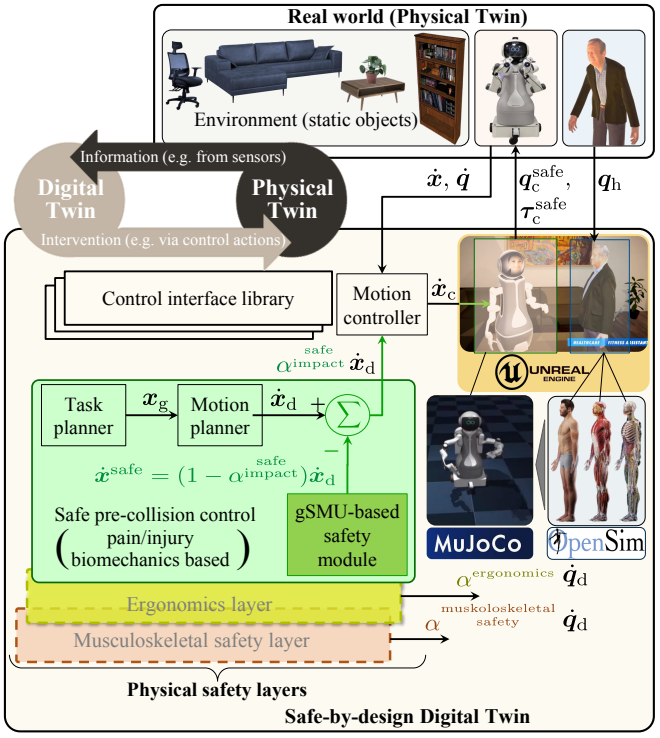

Fig. 2: Safe-by-design digital twin concept. The PT⇌DT interaction framework (top-left) ensures that only safe control actions are applied to physical entities in the real world. The real-time transmission of their actual status information ensures high transparency while allowing for precise synchronization of their simulated avatars. Highlighted layers in transparent boxes outlined with dashed borders will be the focus of our future research.

II. Foundations and System Models

In this section, kinematic structures and dynamic models of the main subsystems of the employed humanoid system are introduced as modular building blocks for its whole-body dynamics. For the sake of clarity and to avoid a cluttered notation, we leave out the dependence of the variables on time t. The fundamental case of rigid links and joint couplings is considered, and a well-known approach for obtaining an unconstrained free representation for the whole-body dynamics of mobile manipulator systems is reviewed and adapted for use with the considered humanoid system.

A. Considered robot systems and their dynamics

We consider a dual-arm humanoid robot that has a differential drive-wheeled mobile base moving its body platform. The geometrical dimensions and inertial parameters of the base platform and body are shown in Tab. I. The active wheels of the base platform are shown in black, and the passive wheels are depicted as gray circles. The active wheels of the differential-drive base can rotate independently from each other while satisfying the conditions of pure rolling and non-slipping. At the locations $\mathcal{L}$, $\mathcal{R}$ on the body platform, two seven-DOF[1] Franka Emika Panda manipulator arms (identical, each has a total weight of 18 kg) are mounted. Also, a third serial rigid link connects the humanoid head to the body platform.[2] The combination of wheeled base, body platform (with its head), and dual-arm manipulator subsystem forms the

[1]DOF is a standard robotics acronym for the motion's ***d**egrees-**o**f-**f**reedom*.
[2]For simplicity and without any loss of generality, we assume the serial link connecting the head to the body to be static, thus, it is considered throughout the paper as a lumped mass added to the body.

wheeled humanoid robot system under consideration. Its generalized coordinates $\boldsymbol{q} \in \mathbb{R}^n$ $(n := n_v + n_l + n_r)$ are composed by the base vehicle coordinates $\boldsymbol{q}_v \in \mathbb{R}^{n_v}$ and the dual-arm manipulator system coordinates $\boldsymbol{q}_l \in \mathbb{R}^{n_l}$ and $\boldsymbol{q}_r \in \mathbb{R}^{n_r}$[3]

$$\boldsymbol{q} = \begin{bmatrix} \boldsymbol{q}_v \\ \boldsymbol{q}_l \\ \boldsymbol{q}_r \end{bmatrix}. \tag{1}$$

The coupled dynamics of this dual-arm wheeled humanoid system can be expressed in the decomposed, modular form

$$\underbrace{\begin{bmatrix} \boldsymbol{M}'_v(\boldsymbol{q}) & \boldsymbol{M}_{vl}(\boldsymbol{q}) & \boldsymbol{M}_{vr}(\boldsymbol{q}) \\ \boldsymbol{M}_{vl}^{\mathsf{T}}(\boldsymbol{q}) & \boldsymbol{M}_l(\boldsymbol{q}_l) & \boldsymbol{0} \\ \boldsymbol{M}_{vr}^{\mathsf{T}}(\boldsymbol{q}) & \boldsymbol{0} & \boldsymbol{M}_r(\boldsymbol{q}_r) \end{bmatrix}}_{\boldsymbol{M}(\boldsymbol{q})} \underbrace{\begin{bmatrix} \ddot{\boldsymbol{q}}_v \\ \ddot{\boldsymbol{q}}_l \\ \ddot{\boldsymbol{q}}_r \end{bmatrix}}_{\ddot{\boldsymbol{q}}} = \underbrace{\begin{bmatrix} \boldsymbol{E}_v(\boldsymbol{q}_v) & \boldsymbol{0}\,\boldsymbol{0} \\ \boldsymbol{0} & \boldsymbol{I}\,\boldsymbol{0} \\ \boldsymbol{0} & \boldsymbol{0}\,\boldsymbol{I} \end{bmatrix}}_{\boldsymbol{\tau}} + \underbrace{\begin{bmatrix} \boldsymbol{A}_v(\boldsymbol{q}_v)^{\mathsf{T}} \boldsymbol{\lambda}_v \\ \boldsymbol{0} \\ \boldsymbol{0} \end{bmatrix}}_{\boldsymbol{\tau}_{\text{con}}}, \tag{2}$$
$$+ \boldsymbol{C}(\boldsymbol{q}, \dot{\boldsymbol{q}}) \dot{\boldsymbol{q}} + \boldsymbol{\tau}_f + \boldsymbol{g}(\boldsymbol{q})$$

where the symmetric, positive definite mass matrix of the coupled system is denoted by $\boldsymbol{M}(\boldsymbol{q}) \in \mathbb{R}^{n \times n}$, the Corilois matrix by $\boldsymbol{C}(\boldsymbol{q}, \dot{\boldsymbol{q}}) \dot{\boldsymbol{q}} \in \mathbb{R}^{n \times n}$ and its defined through the Christoffel symbols of the first kind satisfying $\dot{\boldsymbol{M}}(\boldsymbol{q}) = \boldsymbol{C}(\boldsymbol{q}, \dot{\boldsymbol{q}}) + \boldsymbol{C}^{\mathsf{T}}(\boldsymbol{q}, \dot{\boldsymbol{q}})$, and the gravity torque by $\boldsymbol{g}(\boldsymbol{q}) \in \mathbb{R}^n$. The actuation input transformation matrix is denoted by $\boldsymbol{E}(\boldsymbol{q}) \in \mathbb{R}^{n \times r}$, the input torque vector by $\boldsymbol{\tau} \in \mathbb{R}^n$, the constraint forces by $\boldsymbol{\tau}_{\text{con}} \in \mathbb{R}^n$, and $\boldsymbol{I}$ and $\boldsymbol{0}$ are respectively identity and zero matrices with appropriate dimensions.

Our specific base vehicle subsystem is subject to m constraints, where the matrix associated with them is denoted by $\boldsymbol{A}_v(\boldsymbol{q}_v) \in \mathbb{R}^{m \times n_v}$ and $\boldsymbol{\lambda}_v \in \mathbb{R}^m$ is the vector of constraint forces. The base vehicle's steering always satisfies

$$\dot{\boldsymbol{q}}_v = \boldsymbol{S}(\boldsymbol{q}_v)\, {}^{\mathbb{S}}\dot{\boldsymbol{q}}_v, \tag{3}$$

where $\boldsymbol{S}(\boldsymbol{q}_v)$ is the constraint auxiliary matrix mapping from the space of input velocity ${}^{\mathbb{S}}\dot{\boldsymbol{q}}_v$ to the velocities of the two wheels (i.e., the space of differential coordinates of the wheeled base vehicle) $\dot{\boldsymbol{q}}_v$ [37], [38]. This matrix includes the vehicle's motion constraints (e.g., on the wheels) and fulfills the equality $\boldsymbol{S}^{\mathsf{T}}(\boldsymbol{q}_v) \boldsymbol{A}_v^{\mathsf{T}}(\boldsymbol{q}_v) = \boldsymbol{0}$. In other words, the space spanned by the auxiliary mapping $\boldsymbol{S}(\boldsymbol{q}_v)$ always lies in the nullspace of the constraint $\boldsymbol{A}(\boldsymbol{q}_v)$. Hence, the superscript $\mathbb{S}$ denotes a constraint-free space quantity.

Since the two arms experience no movement constraints,[4] the velocity vector of the full humanoid system is obtained from

$$\dot{\boldsymbol{q}} = \boldsymbol{S}_{\boldsymbol{I}}(\boldsymbol{q}_v)\, {}^{\mathbb{S}}\dot{\boldsymbol{q}} = \begin{bmatrix} \boldsymbol{S}(\boldsymbol{q}_v) & \boldsymbol{0}\,\boldsymbol{0} \\ \boldsymbol{0} & \boldsymbol{I}\,\boldsymbol{0} \\ \boldsymbol{0} & \boldsymbol{0}\,\boldsymbol{I} \end{bmatrix} \begin{bmatrix} {}^{\mathbb{S}}\dot{\boldsymbol{q}}_v \\ \dot{\boldsymbol{q}}_l \\ \dot{\boldsymbol{q}}_r \end{bmatrix}. \tag{4}$$

The corresponding constraint-free velocities can similarly be mapped via an extended Jacobian ${}^{\mathbb{S}}\boldsymbol{J}(\boldsymbol{q}) \in \mathbb{R}^{6 \times n}$ to operational space velocity twist $\dot{\boldsymbol{x}} \in \mathbb{R}^{6 \times 1}$ as

$$\dot{\boldsymbol{x}} = \boldsymbol{J}(\boldsymbol{q})\dot{\boldsymbol{q}} = {}^{\mathbb{S}}\boldsymbol{J}(\boldsymbol{q})\, {}^{\mathbb{S}}\dot{\boldsymbol{q}} = \underbrace{\begin{bmatrix} \boldsymbol{J}_v(\boldsymbol{q}_v)\boldsymbol{S}(\boldsymbol{q}_v) & \boldsymbol{J}_l(\boldsymbol{q}_l) & \boldsymbol{J}_r(\boldsymbol{q}_r) \end{bmatrix}}_{{}^{\mathbb{S}}\boldsymbol{J}(\boldsymbol{q})} \begin{bmatrix} {}^{\mathbb{S}}\dot{\boldsymbol{q}}_v \\ \dot{\boldsymbol{q}}_l \\ \dot{\boldsymbol{q}}_r \end{bmatrix}, \tag{5}$$

where $\boldsymbol{J}_v(\boldsymbol{q}_v) \in \mathbb{R}^{6 \times n_v}$, $\boldsymbol{J}_l(\boldsymbol{q}_l) \in \mathbb{R}^{6 \times n_l}$, $\boldsymbol{J}_r(\boldsymbol{q}_r) \in \mathbb{R}^{6 \times n_r}$ are the Jacobian matrices associated with the mobile base vehicle, the left arm, and the right arm, respectively.

[3]For the considered system, the two manipulation arms are identical both kinematically and dynamically, i.e. $n_l = n_r$.

[4]Except for the obvious actuator and controller interface constraints, defined by the used motors and dictated by the robot manufacturer.

B. Constraint-free whole-body dynamics

As already previously shown in [39], the whole-body coupled dynamics of the dual-arm wheeled humanoid can be derived from the macro/mini structure approach [40]. In the constraint-free space $\mathbb{S}$, its whole-body dynamics can be expressed in the form

$${}^{\mathbb{S}}\boldsymbol{M}(\boldsymbol{q})\, {}^{\mathbb{S}}\ddot{\boldsymbol{q}} + {}^{\mathbb{S}}\boldsymbol{C}(\boldsymbol{q}, \dot{\boldsymbol{q}})\, {}^{\mathbb{S}}\dot{\boldsymbol{q}}_v + {}^{\mathbb{S}}\boldsymbol{g}(\boldsymbol{q}) = {}^{\mathbb{S}}\boldsymbol{\tau}, \tag{6}$$

where

$$\begin{aligned} {}^{\mathbb{S}}\boldsymbol{M}(\boldsymbol{q}) &= \boldsymbol{S_I}^{\mathsf{T}}(\boldsymbol{q}_v) \boldsymbol{M}(\boldsymbol{q}) \boldsymbol{S_I}(\boldsymbol{q}_v) \\ {}^{\mathbb{S}}\boldsymbol{C}(\boldsymbol{q}, \dot{\boldsymbol{q}}) &= \boldsymbol{S_I}^{\mathsf{T}}(\boldsymbol{q}_v) \left(\boldsymbol{M}(\boldsymbol{q}) \dot{\boldsymbol{S}}_{\boldsymbol{I}}(\boldsymbol{q}_v) + \boldsymbol{C}(\boldsymbol{q}, \dot{\boldsymbol{q}}) \boldsymbol{S_I}(\boldsymbol{q}_v) \right) \\ {}^{\mathbb{S}}\boldsymbol{g}(\boldsymbol{q}) &= \boldsymbol{S_I}^{\mathsf{T}}(\boldsymbol{q}_v) \boldsymbol{G}(\boldsymbol{q}), \\ {}^{\mathbb{S}}\boldsymbol{\tau} &= \boldsymbol{S_I}^{\mathsf{T}}(\boldsymbol{q}_v) \boldsymbol{E}(\boldsymbol{q}) \boldsymbol{\tau}. \end{aligned} \tag{7}$$

C. Inertial impact properties and safe pre-collision control

The pseudo-kinetic energy matrix of the system ${}^{\mathbb{S}}\boldsymbol{\Lambda}^{-1}(\boldsymbol{q})$ can be evaluated as

$$\begin{aligned} {}^{\mathbb{S}}\boldsymbol{\Lambda}^{-1}(\boldsymbol{q}) &= {}^{\mathbb{S}}\boldsymbol{J}(\boldsymbol{q})\, {}^{\mathbb{S}}\boldsymbol{M}^{-1}(\boldsymbol{q})\, {}^{\mathbb{S}}\boldsymbol{J}^{\mathsf{T}}(\boldsymbol{q}) \\ &= \begin{bmatrix} {}^{\mathbb{S}}\boldsymbol{\Lambda}_{tr}^{-1}(\boldsymbol{q}) & \overline{{}^{\mathbb{S}}\boldsymbol{\Lambda}_{co}}(\boldsymbol{q}) \\ \overline{{}^{\mathbb{S}}\boldsymbol{\Lambda}_{co}}(\boldsymbol{q})^{\mathsf{T}}(\boldsymbol{q}) & {}^{\mathbb{S}}\boldsymbol{\Lambda}_{rot}^{-1}(\boldsymbol{q}) \end{bmatrix}, \end{aligned} \tag{8}$$

where ${}^{\mathbb{S}}\boldsymbol{\Lambda}_{tr}^{-1}(\boldsymbol{q})$, ${}^{\mathbb{S}}\boldsymbol{\Lambda}_{rot}^{-1}(\boldsymbol{q})$, $\overline{{}^{\mathbb{S}}\boldsymbol{\Lambda}_{co}}(\boldsymbol{q})$ denotes the translational, rotational, and coupling parts of ${}^{\mathbb{S}}\boldsymbol{\Lambda}^{-1}(\boldsymbol{q})$, respectively. Moreover, the reflected mass $m_u(\boldsymbol{q})$ along a Cartesian direction $\boldsymbol{u} \in \mathbb{R}^3$ and the inertia about that direction $I_u(\boldsymbol{q})$, taking into account the base vehicle's motion constraint into account, are given by

$$\begin{aligned} m_{\boldsymbol{u}}(\boldsymbol{q}) &= \left(\boldsymbol{u}^{\mathsf{T}}\, {}^{\mathbb{S}}\boldsymbol{\Lambda}_{tr}^{-1}(\boldsymbol{q})\, \boldsymbol{u} \right)^{-1}, \\ I_{\boldsymbol{u}}(\boldsymbol{q}) &= \left(\boldsymbol{u}^{\mathsf{T}}\, {}^{\mathbb{S}}\boldsymbol{\Lambda}_{rot}^{-1}(\boldsymbol{q})\, \boldsymbol{u} \right)^{-1}. \end{aligned} \tag{9}$$

III. Methodology

This section outlines the key concepts of our proposed safe-by-design Digital Twin (DT). Herein, we elaborate on its core methodology, which includes the DT-guided safety framework for HRI and the real-time synchronized PT⇋DT bidirectional communication approach.

A. DT-guided safety concept for HRI

Since service humanoids are generally expected to operate in human-populated environments, a multitude of safety concerns will typically arise. Addressing those concerns adequately is of paramount importance for any foreseeable integration of such robots, including GARMI, to support humans with everyday tasks. For this, we rely on and extend our recently proposed approach for addressing various safety aspects in HRI [41]. There, on top of ethical, legal, and security aspects, we distinguish the following safety layers

Physical safety layers	Cognitive safety layers
– Impact safety	– Perceived safety
– Ergonomics	– Acceptance
– Musculoskeletal safety	– Personalization

Furthermore, all physical and cognitive safety layers are subject to anthropomorphic scaling and user customizations. For the sake of brevity and to be able to show concrete results proving the feasibility of the proposed safe-by-design

TABLE I: Geometrical schematics and parameters of the considered wheeled humanoid robot GARMI.

Actuated wheels
Mass: 2.9 kg, Radius: 0.08 m
Max. translational velocity: $0.08\,\mathrm{ms}^{-1}$
Inertia about rolling axis: $0.0089\,\mathrm{kgm}^2$
Platform body
Mass: 60 kg (including wheeled base, torso, and head)
Inertia about center of mass: $3.1\,\mathrm{kgm}^2$
Dimensions[m]: $l=1.2\,c=0.5\,b=0.15\,d=0.68\,h=0.19$
Arm base mounting location in base frame [m]:
${}^{\mathcal{V}}\boldsymbol{p}_{\mathcal{L}}=[-0.143,+0.2,+1.129]^{\mathsf{T}}$, ${}^{\mathcal{V}}\boldsymbol{p}_{\mathcal{R}}=[-0.143,-0.2,+1.129]^{\mathsf{T}}$

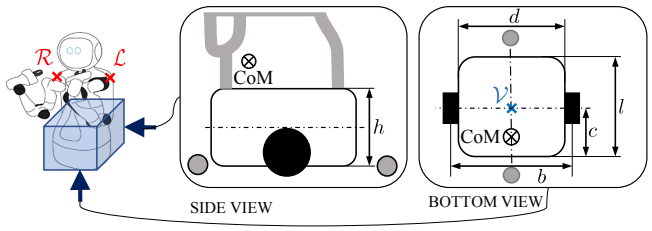

DT-based approach for HRI safety, we limit our discussions through the rest of the paper to physical safety only. Cognitive safety aspects can be well-addressed as high-level constraints on the physical safety layers as already discussed in [41].

Using the generalized Safe Motion Unit (gSMU) pipeline explained in [39], [42], one can also evaluate the inertial properties for assigned points-of-interest (POIs) on both the base and the dual arms along directions of possible impacts with nearby humans. Basically, the gSMU acts as a pain/injury biomechanics based safety filter for planned motions of both the mobile base and the dual arms in the DT, ultimately ensuring their safe pre-collision control in the PT. More specifically, for the reflected masses obtained by the coupled whole-body dynamics (9), the gSMU algorithm ensures a human-safe operation by always producing instantaneous safe velocities along the base body and dual-arm structure. As a result, any desired *risky* base/arm movement, wherein the desired task velocity of at least one POI exceeds the specified safety threshold from the pre-collision safety module, is scaled down. For instance, the impact safety data is typically encoded using pain/injury biomechanics-based safety curves. Therefore, the gSMU shapes the energy of any undesired potential robot-human contact by reducing the task velocity at the robot POI and along the impact direction. Such safety filtering can be achieved, for example, by imposing a scaling factor that satisfies $0\leq\alpha^{\text{safe}}_{\text{impact}}<1$. Similar safety factors can be used to satisfy other physical safety aspects such as, e.g., ergonomics $\alpha^{\text{ergonomics}}$ or musculoskeletal safety $\alpha^{\text{musculoskeletal}}_{\text{safety}}$, see Fig. 2.

B. Real-time synchronization of PT-DT interactions

The key novelty we propose to ensure an effective and safe control for the humanoid robot GARMI involves bridging the gap between the physical world and the digital simulation. This is achieved through the establishment of a seamless real-time "sim-real-sim" loop, wherein the DT simulation remains in constant synchronization with the PT of the real world via sensors, while the desired motion plans are generated in the DT and subsequently transmitted to the PT actuators. Such a transparent PT⇋DT synchronization approach enables precise calibration of the DT and the real-time refinement of the kinematics and dynamics of the simulated systems. These digital systems are developed using a detailed physics engine [43], ensuring physical accuracy with contact-consistent simulated models and control interfaces [44], [45], while continuously mirroring the actual status of the PT. The direct bilateral communication and real-time synchronization for PT⇋DT interactions distinctly enhances transparency in sensing and facilitates a closed-loop control and steering mechanism, setting our digital twin apart from conventional simulation-only methods.

By iterating the required safety evaluations for each point-of-interest (POI) on the robot structure in the DT, only safe task/motion plans and control actions are generated and sent to the real robot for execution as desired trajectories (depending on the level of intervention required), see Fig. 2. Of course, critical safety aspects that do not tolerate any delays, e.g., possibly experienced in the PT⇋DT communication channel, has to be implemented directly on the physical robot (i.e., in the PT) after fulfilling the according sensing requirements. For instance, the gSMU requires at least robust pose tracking of the nearby human(s), which can be addressed via e.g. visual perception. However, the human pose tracking in both PT/DT twins falls outside the scope of of this conceptual work and its video demonstrations. Of course, including the human kinematics and dynamics as well as its tracking are core objectives of our ongoing research using the proposed safe-by-design DT concept.

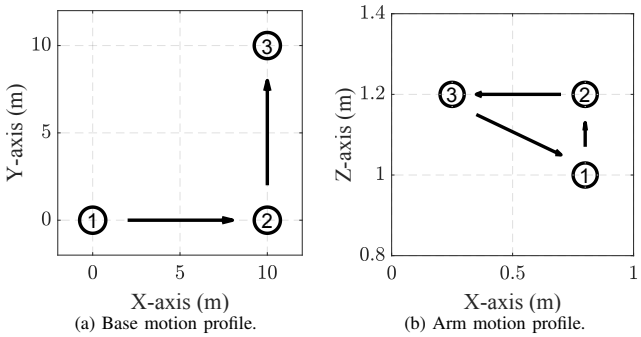

(a) Base motion profile. (b) Arm motion profile.

Fig. 3: Motion profiles for the service robot GARMI. Base followed an L-shaped motion (a), while each arm's end effector performed a triangular motion (b) during the experiments.

C. DT compliance with the GDPR

The analysis of the GDPR requirements for GARMI relies mostly on our previous work [26]. The main result there was the development of a data recorder system [46] that uses encryption, hashing and signing algorithms for the recorded data to ensure transparency, data security and integrity required for compliance with the EU GDPR act [47]. Further details on how the data recorder system was integrated within the proposed digital twin environment can be found in [27].

IV. Experimental Validation

The experimental setup to test the developed DT solution consisted of three main parts connected through ROS[5] as an underlying communication channel:

i) The GARMI robot's physical model that runs in the MuJoCo physics engine [43] while following the motion profiles depicted in Fig. 3a for the base and Fig. 3b for both arms separately.

[5]ROS stands for **R**obot **O**perating **S**ystem, https://www.ros.org/

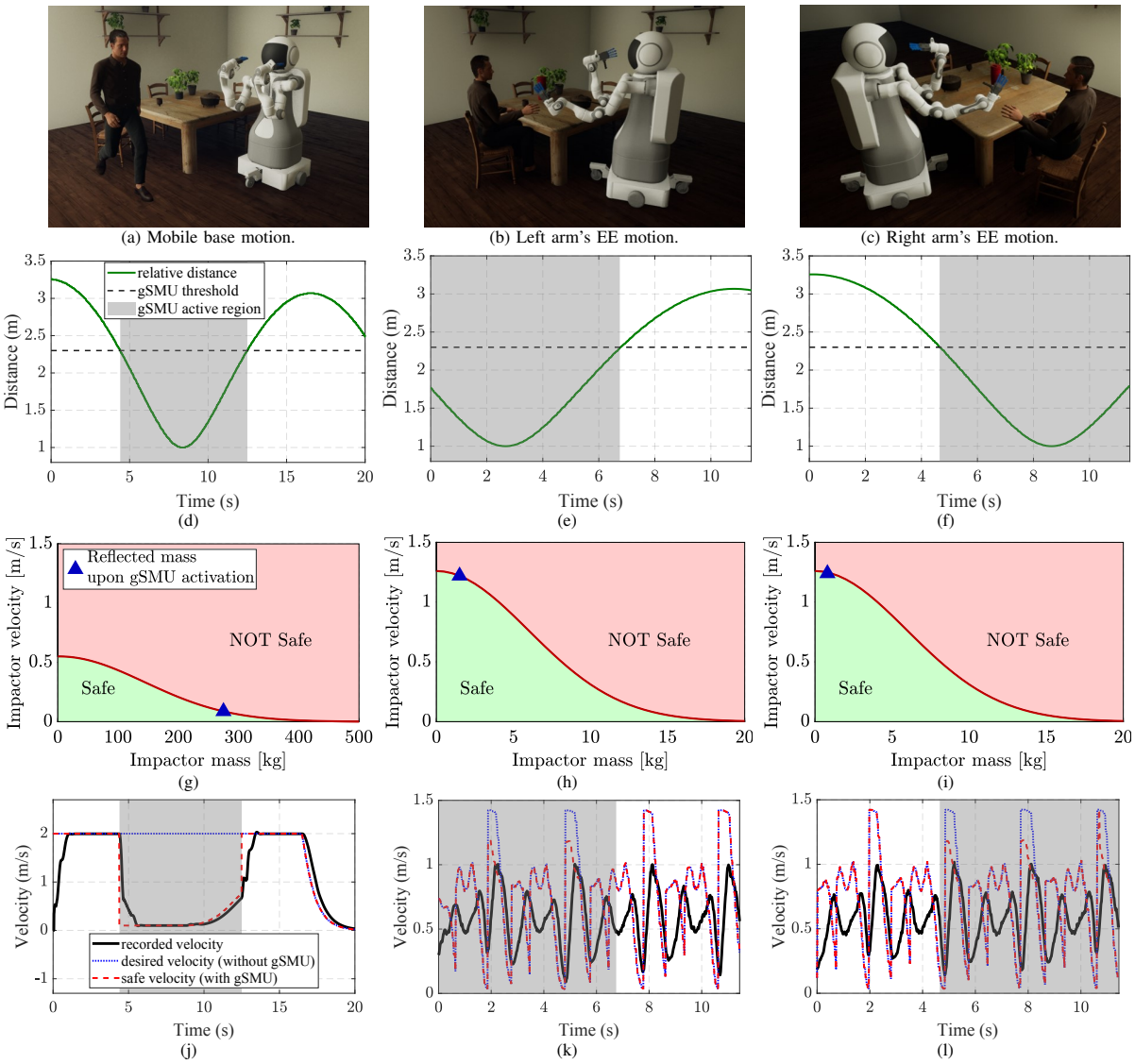

Fig. 4: Results of the gSMU-based impact safety module tested in the DT environment. Each column shows the results for individual analyzed parts of the humanoid, and they report from left to right about the wheeled base, the left arm, and the right arm, respectively. Subplots (a–c) are snapshots from the DT at the time instant when the gSMU safe velocity scaling takes effect. Subplots (d–f) show the relative distances between the robot parts and the human during the experiments. Subplots (g–i) are the underlying safety curves for the respective robot part. Subplots (j–l) depict the effect of the gSMU-based impact safety module on the robot velocities.

ii) The human kinematic model and the environment, which have been simulated using UE5[6] for graphics visualization (see Fig. 2). We employed a sinusoidal function as the relative distance profile between GARMI and the simulated human. Please note that realistic human body kinematics were not considered in this work, however, they are the subject of our ongoing and future research. The distance information was updated with a frequency of 100 Hz. To capture the entire HRI scenario, GARMI's states were visualized in UE5 by interfacing with GARMI's physical model within MuJoCo.

iii) Finally, the gSMU-based safety module that is utilized to adjust velocity commands based on encoded biomechanical impact data and the current states of both the robot and the human. The safety module is activated when the relative robot-human distance falls below 2.3 meters. This distance threshold was chosen heuristically as the protective separation distance $S_p(t_0)$ [11] for the nominal settings of the demonstrated tasks with a simulated human motion of a maximum speed of almost 2 $\mathrm{m/s}$.[7]

To validate the gSMU framework for ensuring the safety of the humanoid robot GARMI, a total of three experiments have been conducted with the DT: one for the base platform and one for the individual arms of GARMI. In the first experiment, the robot base moved following the points shown in Fig. 3a while trying to maintain its maximum velocity of 2 m/s. On the other hand, the end-effector of each GARMI's arm followed the motion profile shown in Fig. 3b.

A. Results

The carried out experiments can be seen in the supplementary video[8] and their results are shown in Fig. 4. The the re-

[6]UE5 stands for **U**nreal **E**ngine 5, https://www.unrealengine.com/en-US

[7]For exemplary calculations of $S_p(t_0)$ relevant to a typical collaborative task with a lightweight robot arm, the reader is advised to check [48].

[8]https://youtu.be/7rHItLRsGyY

sults in the following order: base motion (left), left arm motion (middle), and right arm motion (right). The moments at which the safety module has been triggered causing to scale down the velocity of the moving part are depicted in Fig. 4a–4c. The relative robot-human distances at any given time instant are shown in Fig. 4d–4f. Indicated there as well (highlighted in gray) are the time during which the gSMU module is activated, where the relative robot-human distance falls below a safe distance threshold. The used 2D safety curves in the impactor's mass/velocity plane for the gSMU are displayed in Fig. 4g–4i for using injury biomechanics information from experimental impacts with lower and upper human extremities (for use with the GARMI's base and dual arms, respectively). Lastly, in Fig. 4j–4l the comparisons between the desired velocities, safe velocities, and actual recorded velocities of the part in motion are shown. The forward velocity of the base during the motion is shown in Fig. 4j, whereas the magnitudes of end-effector velocity in task space for the left and right arm are shown in Fig. 4j and Fig. 4l, respectively.

V. Discussion

Results for different use cases were shown in the previous section. In the first experiment, the base of the humanoid was commanded to drive along a path with a constant speed of 2 m/s, however, at this speed, human safety is endangered. Therefore, the humanoid service robot GARMI must slow down when it encounters a human. An example of such a scenario can be seen in Fig. 3a. From the recorded velocity profile shown in Fig. 4j, it is clear that the platform slowed down drastically, thanks to the gSMU framework when triggered by a human. Afterward, when the human has moved away from GARMI, the integrated safety module in DT allows for a slow increase in speed until the human is outside of the gSMU safe distance threshold.

The other two experiments were very similar to each other since they included the same components. The gSMU-based safety module slows down the end-effector movement (see Fig. 4k and Fig. 4l, highlighted area). The important thing to notice there is that the end-effector movement is only restricted when it moves from point 3 to point 1 (Fig. 3b). This feature of the gSMU-based safety module is essential since it only restricts movements in dangerous directions while the robot can move freely in all other directions. This restriction on the velocity scaling is important as it does not compromise the movement efficiency of the robot entirely when a human is nearby.

Regarding the underlying injury biomechanics information employed for safety in our simulated use cases, Fig. 4g–4h display the safety curves that have been used for the safe velocity scaling by the gSMU. The blue triangle indicates the reflected mass for each component when the safety modules get triggered, i.e. when the human gets too close to the robot. For the case of individual arms, the reflected mass is close to $\sim$1 kg. The relatively low value compared to the size and overall weight of the used serial manipulator in the dual-arm system of GARMI (namely, the Franka Emika Panda arm) can be explained by the configurations of the arms while executing their respective tasks (see Fig. 4b and Fig. 4c). During the experiments, the first three joints were mostly stationary while the remaining ones (i.e., the last four joints) contributed the most to achieving the goal positions. Due to their lighter design, these last four joints contribute less to the reflected mass compared to if the first three joints were instructed to move.

All the aforementioned results have been obtained in a DT environment, which provides a simple and inexpensive testing solution for various scenarios that cannot be performed in real life due to the potential risks. Our results show the effectiveness and importance of the novel safe-by-design DT concept that can be implemented and used for prototyping and actual control of complex humanoid robots. Additionally, to ensure safe pHRI, the requirements from relevant safety standards and technical specifications can be also included in the developed DT solution such that the relevant safety aspects of planned robot motions/interactions with humans are adequately analyzed.

VI. Conclusion

This paper presented a safe-by-design DT solution that extends the state-of-the-art digital twin based approaches to address real-world integration challenges of complex robotic systems. Specifically, we considered the use case of a humanoid service robot operating in domestic settings, where we focused on addressing the physical safety aspects of HRI. The results obtained from simulating multiple scenarios that are typical for such service robots moving in a home-like human environment validate the proposed safety-driven DT approach. The integration of detailed human and robot physical models within the DT framework offers several significant advantages in terms of safety tests and validations, overcoming safety issues of service robots. Compared to the risky and potentially more expensive approach of testing directly in the real world, it provides a cost-effective solution for prototyping applications involving physical interaction. This also enables the generation of nominal data sets, encoding potential human-robot interaction patterns, and other key useful task dynamics. For instance, it facilitates the simulation of HRI scenarios and further allows for the investigation of human comfort and ergonomics. Future work may involve the integration of in-vitro human kinematics, musculoskeletal and skin tissue models to further enhance human simulations. Furthermore, the proposed PT$\rightleftharpoons$DT integration scheme offers the potential for improving human models by incorporating sensed and tracked motions into the simulation while also enabling the feedback of simulated robot plans to the actual robot. This tight sense-and.-act interconnection closes the loop between simulation and the real world, enhancing the capabilities and applicability of the developed DT framework.

Acknowledgment

The authors would like to thank V. Rakcevic for his support, discussions and recommendations regarding the adaptation of the gSMU algorithm for use with the humanoid service robot GARMI.

This work was supported by the funding of the Lighthouse Initiative Geriatronics by LongLeif GaPa gGmbH (Project Y), StMWi Bayern (Project X, grant no. IUK-1807-0007// IUK582/001) and, the Bavarian Institute for Digital Transformation (bidt-Project Responsible Robotics RR-AI), the Bavarian State Ministry for Economic Affairs, Regional Development and Energy (StMWi) as part of the project SafeRoBAY (grant number: DIK0203/01), the Federal Ministry of Education and Research of Germany (BMBF) in the programme of "Souverän. Digital. Vernetzt." Joint project 6G-life, project identification number 16KISK002, and the European Union's Horizon 2020 research and innovation program as part of the project DARKO (grant no. 101017274).

REFERENCES

[1] I. O. for Standardization (ISO), "ISO 8373:2021 – Robots and robotic devices - Vocabulary," 2021.

[2] I. González Alonso, M. Fernández, J. M. Maestre, M. d. P. A. García Fuente, and I. G. Alonso, "Service robotics," *Service Robotics within the Digital Home: Applications and Future Prospects*, pp. 89–114, 2011.

[3] K. S. Jones and E. A. Schmidlin, "Human-robot interaction: toward usable personal service robots," *Reviews of Human Factors and Ergonomics*, vol. 7, no. 1, pp. 100–148, 2011.

[4] M. J. Matarić and B. Scassellati, "Socially assistive robotics," *Springer Handbook of Robotics*, pp. 1973–1994, 2016.

[5] L. Van Aerschot and J. Parviainen, "Robots responding to care needs? A multitasking care robot pursued for 25 years, available products offer simple entertainment and instrumental assistance," *Ethics and Information Technology*, vol. 22, no. 3, pp. 247–256, 2020.

[6] A. K. Pandey and R. Gelin, "A mass-produced sociable humanoid robot: Pepper: The first machine of its kind," *RAM*, vol. 25, no. 3, pp. 40–48, 2018.

[7] C. Fattal, I. Cossin, F. Pain, E. Haize, C. Marissael, S. Schmutz, and I. Ocnarescu, "Perspectives on usability and accessibility of an autonomous humanoid robot living with elderly people," *Disability and Rehabilitation: Assistive Technology*, pp. 1–13, 2020.

[8] S. Saeedvand, M. Jafari, H. S. Aghdasi, and J. Baltes, "A comprehensive survey on humanoid robot development," *The Knowledge Engineering Review*, vol. 34, p. e20, 2019.

[9] I. O. for Standardization (ISO), "ISO 10218-1:2011 – Robots and robotic devices - Safety requirements for industrial robots - Part 1: Robots," 2011.

[10] ——, "ISO 10218-2:2011 – Robots and robotic devices - Safety requirements for industrial robots - Part 2: Robot systems and integration," 2011.

[11] ——, "ISO/TS 15066:2016 – Robots and robotic devices – Collaborative robots," 2016.

[12] ——, "ISO 13482:2014 – Robots and robotic devices - Safety requirements for personal care robots," 2014.

[13] P. Salvini, D. Paez-Granados, and A. Billard, "On the safety of mobile robots serving in public spaces: Identifying gaps in EN ISO 13482: 2014 and calling for a new standard," *ACM Trans. on Human-Robot Interaction (THRI)*, vol. 10, no. 3, pp. 1–27, 2021.

[14] ——, "Safety Concerns Emerging from Robots Navigating in Crowded Pedestrian Areas," *Intl. Journal of Social Robotics*, vol. 14, no. 2, pp. 441–462, 2022.

[15] D. Paez-Granados and A. Billard, "Crash test-based assessment of injury risks for adults and children when colliding with personal mobility devices and service robots," *Scientific reports*, vol. 12, no. 1, pp. 1–12, 2022.

[16] A. Martinetti, P. K. Chemweno, K. Nizamis, and E. Fosch-Villaronga, "Redefining safety in light of human-robot interaction: A critical review of current standards and regulations," *Frontiers in chemical engineering*, vol. 3, p. 32, 2021.

[17] H. Iwata and S. Sugano, "Design of human symbiotic robot TWENDY-ONE," in *ICRA*, 2009, pp. 580–586.

[18] R. Kittmann, T. Fröhlich, J. Schäfer, U. Reiser, F. Weißhardt, and A. Haug, "Let me introduce myself: I am Care-O-bot 4, a gentleman robot," *Mensch und computer 2015–proceedings*, 2015.

[19] J. Pages, L. Marchionni, and F. Ferro, "TIAGo: the modular robot that adapts to different research needs," in *International workshop on robot modularity, IEEE/RSJ Intl. Conf. on Intelligent Robots and Systems (IROS)*, vol. 290, 2016.

[20] S. Shigemi, *ASIMO and Humanoid Robot Research at Honda*. Springer Netherlands, 1 2018, pp. 55–90.

[21] T. Asfour, L. Kaul, M. Wächter, S. Ottenhaus, P. Weiner, S. Rader, R. Grimm, Y. Zhou, M. Grotz, F. Paus *et al.*, "Armar-6: A collaborative humanoid robot for industrial environments," in *IEEE/RAS Intl. Conf. on Humanoid Robots*, 2018, pp. 447–454.

[22] M. Fuchs, C. Borst, P. R. Giordano, A. Baumann, E. Kraemer, J. Langwald, R. Gruber, N. Seitz, G. Plank, K. Kunze *et al.*, "Rollin' Justin – Design considerations and realization of a mobile platform for a humanoid upper body," in *ICRA*, 2009, pp. 4131–4137.

[23] M. Schwarz, C. Lenz, A. Rochow, M. Schreiber, and S. Behnke, "Nimbro avatar: Interactive immersive telepresence with force-feedback telemanipulation," in *IROS*. IEEE, 2021, pp. 5312–5319.

[24] M. Tröbinger, C. Jähne, Z. Qu, J. Elsner, A. Reindl, S. Getz, T. Goll, B. Loinger, T. Loibl, C. Kugler *et al.*, "Introducing GARMI – A service robotics platform to support the elderly at home: Design philosophy, system overview and first results," *RAL*, vol. 6, no. 3, pp. 5857–5864, 2021.

[25] Y. Tong, H. Liu, and Z. Zhang, "Advancements in Humanoid Robots: A Comprehensive Review and Future Prospects," *IEEE/CAA Journal of Automatica Sinica*, vol. 11, no. 2, pp. 301–328, 2024.

[26] J. Skerlj, M. Braun, S. Witz, S. Breuer, M. Bak, S. Scholz, A. Naceri, R. Müller, S. Haddadin, and I. Eisenberger, "Data Recording for Responsible Robotics," in *IEEE Intl. Conf. on Advanced Robotics and Its Social Impacts (ARSO)*, 2023, pp. 103–109.

[27] J. Skerlj, D. Pérez-Suay, S. Knebel, H. Sadeghian, A. Naceri, and S. Haddadin, "Virtual reality-based framework for service robotics: Data monitoring and recording during rehabilitation scenarios," *IFAC PapersOnLine*, vol. 56, no. 2, pp. 7044–7051, 2023.

[28] J. Bessler, G. B. Prange-Lasonder, L. Schaake, J. F. Saenz, C. Bidard, I. Fassi, M. Valori, A. B. Lassen, and J. H. Buurke, "Safety assessment of rehabilitation robots: A review identifying safety skills and current knowledge gaps," *Frontiers in Robotics and AI*, p. 33, 2021.

[29] W. Kritzinger, M. Karner, G. Traar, J. Henjes, and W. Sihn, "Digital Twin in manufacturing: A categorical literature review and classification," *IFAC PapersOnLine, IFAC Symposium on Information Control Problems in Manufacturing (INCOM)*, vol. 51, no. 11, pp. 1016–1022, 2018.

[30] Y. H. Son, G.-Y. Kim, H. C. Kim, C. Jun, and S. D. Noh, "Past, present, and future research of digital twin for smart manufacturing," *Journal of Computational Design and Engineering*, vol. 9, no. 1, pp. 1–23, 2022.

[31] M. W. Grieves, "Digital Twins: Past, Present, and Future," in *The Digital Twin*. Springer, 2023, pp. 97–121.

[32] C. Semeraro, M. Lezoche, H. Panetto, and M. Dassisti, "Digital twin paradigm: A systematic literature review," *Computers in Industry*, vol. 130, p. 103469, 2021.

[33] L. Cascone, M. Nappi, F. Narducci, and I. Passero, "DTPAAL: Digital twinning pepper and ambient assisted living," *IEEE Trans. on Industrial Informatics*, vol. 18, no. 2, pp. 1397–1404, 2021.

[34] T. Maruyama, T. Ueshiba, M. Tada, H. Toda, Y. Endo, Y. Domae, Y. Nakabo, T. Mori, and K. Suita, "Digital twin-driven human robot collaboration using a digital human," *Sensors*, vol. 21, no. 24, p. 8266, 2021.

[35] A. K. Ramasubramanian, R. Mathew, M. Kelly, V. Hargaden, and N. Papakostas, "Digital twin for human–robot collaboration in manufacturing: Review and outlook," *Applied Sciences*, vol. 12, no. 10, p. 4811, 2022.

[36] V. Weistroffer, F. Keith, A. Bisiaux, C. Andriot, and A. Lasnier, "Using physics-based digital twins and extended reality for the safety and ergonomics evaluation of cobotic workstations," *Frontiers in Virtual Reality*, vol. 3, p. 781830, 2022.

[37] Y. Yamamoto and X. Yun, "Coordinating locomotion and manipulation of a mobile manipulator," in *CDC*, 1992, pp. 2643–2648.

[38] J. Barraquand and J.-C. Latombe, "Nonholonomic multibody mobile robots: Controllability and motion planning in the presence of obstacles," *Algorithmica*, vol. 10, no. 2-4, pp. 121–155, 1993.

[39] M. Hamad, A. Kurdas, N. Mansfeld, S. Abdolshah, and S. Haddadin, "Modularize-and-Conquer: A Generalized Impact Dynamics and Safe Precollision Control Framework for Floating-Base Tree-Like Robots," *TRO*, 2023.

[40] O. Khatib, "Inertial properties in robotic manipulation: An object-level framework," *The international journal of robotics research*, vol. 14, no. 1, pp. 19–36, 1995.

[41] M. Hamad, S. Nertinger, R. J. Kirschner, L. Figueredo, A. Naceri, and S. Haddadin, "A Concise Overview of Safety Aspects in Human-Robot Interaction," *Human-Friendly Robotics (HFR) Workshop 2023, Springer Proceedings In Advanced Robotics*, vol. 25, 2024, [Accepted].

[42] S. Haddadin, S. Haddadin, A. Khoury, T. Rokahr, S. Parusel, R. Burgkart, A. Bicchi, and A. Albu-Schäffer, "On making robots understand safety: Embedding injury knowledge into control," *IJRR*, vol. 31, no. 13, pp. 1578–1602, 2012.

[43] E. Todorov, T. Erez, and Y. Tassa, "Mujoco: A physics engine for model-based control," in *IROS*, 2012, pp. 5026–5033.

[44] J. Elsner, G. Reinerth, L. Figueredo, A. Naceri, U. Walter, and S. Haddadin, "PARTI-A Haptic Virtual Reality Control Station for Model-Mediated Robotic Applications," *Frontiers in Virtual Reality*, vol. 3, 2022.

[45] J. Elsner, "Taming the Panda with Python: A powerful duo for seamless robotics programming and integration," *SoftwareX*, vol. 24, p. 101532, 2023.

[46] A. F. T. Winfield and M. Jirotka, "The Case for an Ethical Black Box," in *Towards Autonomous Robotic Systems*, Y. Gao, S. Fallah, Y. Jin, and C. Lekakou, Eds. Cham, Germany: Springer International Publishing, 2017, pp. 262–273.

[47] "The European General Data Protection Regulation (GDPR)," European Commission, 2018. [Online]. Available: https://gdpr-info.eu/

[48] P. Svarny, M. Tesar, J. K. Behrens, and M. Hoffmann, "Safe physical HRI: Toward a unified treatment of speed and separation monitoring together with power and force limiting," in *IROS*, 2019, pp. 7580–7587.